ROYAL SOCIETY
OF CHEMISTRY

PAPER

Check for updates

Electrical-pumping spasing action from cross-stacked microwires†

Zhanguo Li,[ab] Gaohang He,[c] Mingming Jiang, ID *[ad] Jiaolong Ji,[d] Chongxin Shan*[ae] and Dezhen Shen*[a]

The realization of electrically pumped lasers at deep sub-micro and nanometer scale operating far beyond the diffraction limit is still a crucial goal in nanophotonics and plasmonics for prospective fundamental research and application. Herein, electrically pumped spasing action was captured from a cross-stacked architecture composed of a single Ga-doped ZnO microwire (ZnO:Ga MW) crossed with another ZnO:Ga MW covered by Au nanoparticles. To exploit the spasing feature, a plasmonic nanocavity could be constructed based on the sandwiched structures, with isolated Au nanoparticles filling the spacer between the crossed MWs. When both emission regions from the crossed MWs overlapped with each other, the cross-stacked architecture exhibited quasi-Schottky junction behavior, resulting in the formation of a tunneling junction. When the injection current exceeded certain values, bright and localizing emissions were observed at the crossed regions, with a sharp peak emerging in the emission spectra. The dominant emission wavelengths centered at 550 nm were accompanied by the spectral linewidth rapidly narrowing to 2 nm, suggesting a transition from spontaneous to stimulated emission. The electrically pumped lasing characteristics can be attributed to efficient metal plasmons amplification by the stimulated emission of radiation from Au nanoparticles, which filled the nanocavities. Therefore, this cross-stacked architecture provides a natural route towards electrical injection schemes that can be employed to construct electrical-pumping spasers. This technology also provides a candidate to investigate the fabrication of tunneling diodes.

1 Introduction

Due to well-crystallized, excellent optical gain behavior, and outstanding electronic transport characteristics, numerous studies have been carried out to explore one-dimensional (1D) structures as eye-catching illumination and design elements to construct sophisticated light-emitting diodes, lasers, and other optoelectronic devices. For instance, cross-stacked nanowires (NWs) junction arrays can provide a generic possibility for the fabrication of high-density integrated devices with an individual addressable function at each cross point.[1–5] An assembly of semiconducting III–V and II–VI NWs used to produce integrated photonic and electronic–photonic systems have been reported, affording enormous potential applications in photovoltaic/detection systems, information storage, photonic integrated circuits, and so on.[6–10] Realizing these multifunctional applications will require building blocks with tunable electronic transport properties and wavelength-tunable emissions that can be rationally achieved and integrated into optoelectronic devices.[11–15] Central to realizing actively tunable device components is the rational control of key material parameters, such as chemical composition, structure, size, morphology, doping, and so on. It is these parameters that determine, for example, electronic and optoelectronic properties critical for predictable device diverse functionality.[16–20]

In addition, metal nanostructures have been extensively studied for their unique ability to focus light into nanometer-scale volumes due to the large localized electromagnetic fields. One of the key functions for the exploitation of the plasmonic effect is an efficient conversion of plasmon energy into an electrical signal or *vice versa*.[21–25] Metal–semiconductor hybrid structures enable plasmonic energy detection as a platform to dominate electrical currents. Photons absorbed in a metal nano-structure can generate hot electrons, and then, in turn, the electrons can cross the boundary between metal and semi-conductor by thermionic diffusion, resulting in photocurrent

[a] *State Key Laboratory of Luminescence and Applications, Changchun Institute of Optics, Fine Mechanics and Physics, Chinese Academy of Sciences, No. 3888 Dongnanhu Road, Changchun, 130033, China. E-mail: shendz@ciomp.ac.cn*

[b] *University of Chinese Academy of Sciences, Beijing 100049, China*

[c] *Vacuum Interconnected Nanotech Workstation, Suzhou Institute of Nano-Tech and Nano-Bionics, Chinese Academy of Sciences, Suzhou 215123, China*

[d] *College of Science, Nanjing University of Aeronautics and Astronautics, No. 29 Jiangjun Road, Nanjing 210016, China. E-mail: mmjiang@nuaa.edu.cn*

[e] *School of Physics and Engineering, Zhengzhou University, Zhengzhou 450001, China. E-mail: cxshan@zzu.edu.cn*

† Electronic supplementary information (ESI) available. See DOI: 10.1039/c9tc03537k

This journal is © The Royal Society of Chemistry 2019

J. Mater. Chem. C, 2019, 7, 10933–10944 | **10933**

enhancement, or energy band modification in semiconductors.[26–29] Consequently, such hybrid architectures have been proposed as efficient components that can be integrated into electronic and optoelectronic devices to considerably enhance the performance of conventional optoelectronic devices, such as photovoltaic and photocatalytic devices, photoelectric detectors, light-emitting devices and lasers and so on.[28–31] Taking metal nanostructures-based microsized emitters for instance, their excited states could be coupled with metal plasmons at metal–semiconductor interfacial contact regions, where local field enhancement can lead to an increase in brightness and emission regions. Thus, the electrical excitation and detection of localized surface plasmons offer dramatic advantages over standard coupling schemes, which can be used to construct novel light sources and displays based on metal–semiconductor hybrid architectures. However, the realization of electrically driven generation of non-equilibrium hot electrons through plasmonic decay nonradiatively from metal nanostructures, as well as hot electrons induced light-emitting devices, remains in its infancy.[23,24,32]

In this work, a cross-stacked architecture composed of a single bare Ga-doped ZnO microwire (ZnO:Ga MW), crossed with another ZnO:Ga MW prepared with Au nanoparticles decoration (AuNPs@ZnO:Ga) was constructed. By applying bias onto the crossed MWs simultaneously, bright and localized emissions can be recorded, with the emission areas located towards the crossing region. Especially, when the injection current exceeded beyond certain thresholds, single sharp emission peaks emerged on the emission spectra. The dominating emission wavelengths centered at 550 nm, accompanied with a spectral linewidth that quickly narrowed to be 2 nm. To characterize the emission features, the cross-stacked architecture exhibited quasi-Schottky behavior, suggesting the formation of a tunneling junction between the ZnO:Ga–AuNPs–ZnO:Ga based sandwiched structure. Meanwhile, physically isolated Au nanoparticles aggregated and sandwiched into the crossed regions could be used to construct plasmonic nanocavities together with the smooth surfaces f the crossed MWs serving as the feedback mirrors, resulting in Au-plasmon amplification by stimulated inelastic tunneling electrons from the sandwiched and aggregated Au nanoparticles. Therefore, electrically pumped spasing behavior can be achieved on account of the cross-stacked architectures. Therefore, the hybrid architecture can provide potential applications in the fabrication of electrical spasers, hot-electron induced multicolored light sources and tunneling diodes, electronic transport modulation, *etc.*

2 Experimental section

Quartz pieces with a size of 4 × 4 cm were adopted as the substrate. Subsequently, the single MW was selected to fabricate the metal–semiconductor–metal (MSM) structures based filament-type emitter, with indium (In) particles serving as the electrodes. By means of a radio-frequency magnetron sputtering technique, Au (99.99%) quasiparticle nanofilm was evaporated on the ZnO:Ga MW. Thus, the single ZnO:Ga MW prepared with Au

quasiparticle nanofilm deposition (Au@ZnO:Ga) based MSM structure was also fabricated, as shown in Fig. S1 in the ESI.† [33,34] Additionally, increasing the sputtering time can be employed to modulate the thickness of the evaporated metal quasiparticle nanofilms. When the bias applied onto both ends of the MW reached a certain value, light-emitting can be observed. After maintaining for about 5 min, the quasiparticle nanofilms can be transferred into isolated nanoparticles towards the lighting regions due to the Joule heating effect. Thus, a typical incandescent light source composed of a single ZnO:Ga MW covered with isolated Au nanoparticles (AuNPs@ZnO:Ga) was prepared. Additionally, the fabrication of the cross-stacked architecture involving a single ZnO:Ga MW crossed with another AuNPs@ZnO:Ga MW was fabricated as follows: firstly, the brightest emission regions from the single AuNPs@ZnO:Ga MW should be marked; secondly, the other single ZnO:Ga MW was then selected and transferred to cross over the AuNPs@ZnO:Ga MW, with the contact zone overlapped at the emission region marked previously. Finally, the crossed MWs were fixed by In particles. To guarantee that the emission regions from the crossed MWs overlapped with each other, another quartz plate (size: 3 × 3 cm) was utilized to put pressure on the contact zone, leading to an excellent contact between the crossed MWs.

3 Results and discussion

3.1 Optical and electrical properties of single ZnO:Ga MWs prepared *via* Au quasiparticle nanofilm decoration

Synthesis of ZnO and ZnO:Ga MWs: individual ZnO MWs (weight ratio of ZnO : graphite (C) = 1 : 1) and ZnO:Ga MWs (weight ratio of $ZnO : Ga_2O_3 : C = 10 : 1 : 11$) were synthesized *via* a one-step chemical vapor deposition method.[12,13,33,35] The as-synthesized ZnO MW and ZnO:Ga MW were characterized using scanning electron microscopy (SEM), as shown in Fig. 1(a) and (b). From the insets, one can observe that the MWs possessed perfect hexagonal cross-sections. To verify that the Ga species is being incorporated into the ZnO crystal lattice, elemental mapping of the Zn, O and Ga species was performed using energy dispersive X-ray spectroscopy (EDX) mapping, as shown in Fig. 1(c). The EDX mapping within the spatial resolution demonstrated that Ga-incorporation distribution was uniform throughout the MW.[12,34,35]

To probe into the influence of Ga-incorporation on the optical properties, photoluminescence (PL) emission measurement of the single ZnO MW was carried out and showed a predominant ultraviolet emission centered at 381 nm, together with a weaker visible emission, as demonstrated in Fig. 1(d). Meanwhile, the electrical conduction characteristics of the single ZnO MW was also carried out, as shown in the inset of Fig. 1(d). In contrast, PL measurements of single ZnO:Ga MWs prepared with and without Au quasiparticle nanofilm decoration exhibited a typical ultraviolet near-band edge (NBE) emission centered at approximately 376 nm that dominated the PL emission, as displayed in Fig. 1(e). By introducing Au quasiparticle nanofilm evaporation with the sputtering time ranging
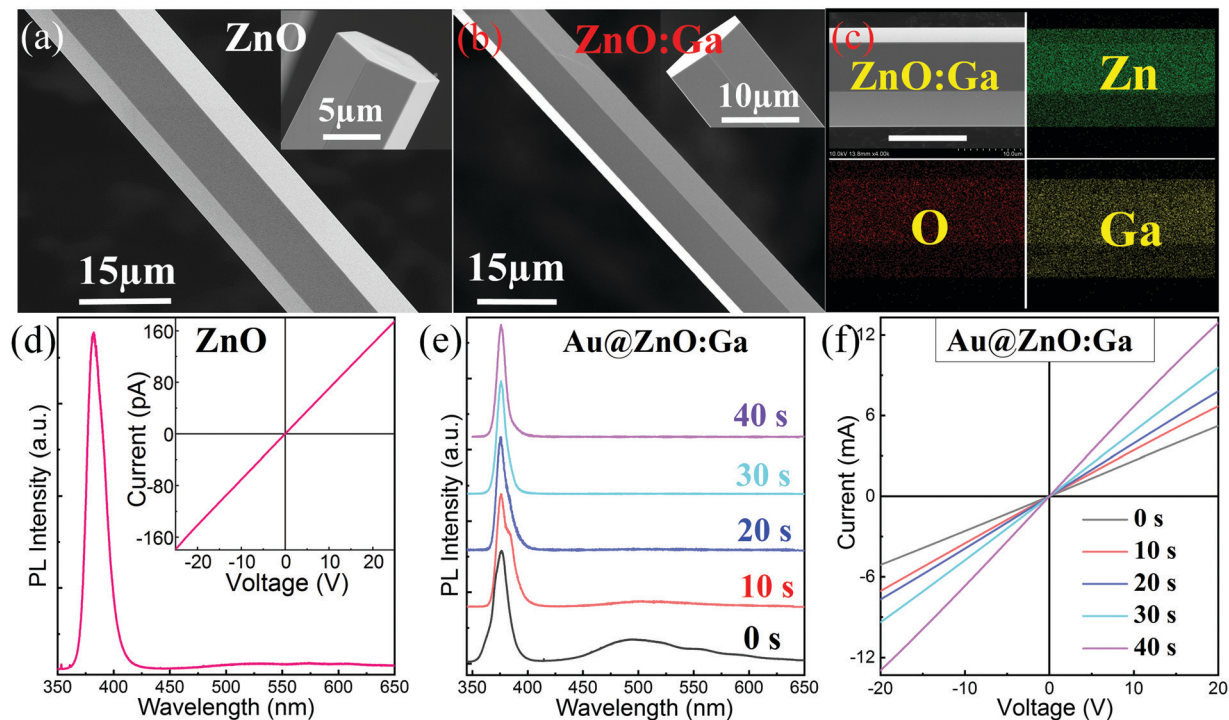
10934 | *J. Mater. Chem. C,* 2019, **7**, 10933–10944

This journal is © The Royal Society of Chemistry 2019

Fig. 1 (a) SEM image of as-synthesized single ZnO MW, with perfect hexagonal cross section shown in the inset. (b) SEM image of single ZnO:Ga MW, with perfect hexagonal cross section exhibited in the inset. (c) EDX mapping of Zn, O, and Ga species distribution (scale bar: 10 μm). (d) PL spectrum of single ZnO MW, with the $I–V$ characteristics shown in the inset. (e) PL emission spectra of single ZnO:Ga MW prepared without and with Au quasiparticle nanofilm evaporation, with the sputtering time ranging from 0 to 40 s. (f) $I–V$ characteristics curves of single ZnO:Ga MW prepared without and with Au quasiparticle nanofilm decoration, with the sputtering time ranging from 0 to 40 s.

from 0 s to 40 s, the ratio between the NBE-type emission and visible emission can be further enhanced. Thus, the incorporation of Au quasiparticle nanofilm deposition on the ZnO:Ga MW can be utilized to improve the optical properties of the single ZnO:Ga MW. Due to the Ga incorporation, electronic transport measurements from the single ZnO:Ga MW indicated that n-type conductance can be greatly improved. Especially, by adjusting the sputtering times for the Au quasiparticles nanofilms, the n-type conductance can be further tuned. Therefore, the experimental results directly demonstrated that increasing the sputtering time of the metal quasiparticle nanofilm can also be utilized to improve n-type conduction, accompanied with current–voltage ($I–V$) characteristic curves demonstrated in Fig. 1(f).[13,16,17,34,36]

3.2 EL emission characteristics from single AuNPs@ZnO:Ga MW based incandescent-type emitter

As previously reported, incandescent-type light sources have been realized based on individual ZnO:Ga MWs. By adjusting Ga-incorporation concentration, the dominant lighting wavelengths can be tuned from the visible to near-infrared spectral regions.[12,34,35] Several ZnO:Ga MWs with different Ga-doping concentrations were selected to construct one-dimensional incandescent light sources (detailed information on the emissions can be seen in Fig. S2–S4 in the ESI†). The emitted photons displayed green-lighting, green-yellow lighting, yellow-lighting and red-lighting, respectively. Then, by introducing Au quasiparticle

nanofilms deposition, the modulation of light-emission features can be achieved.[13,33] Taking the sputtering time of 60 s for instance, the $I–V$ characteristics presented a linear and symmetric shape, indicating the ohmic contact formed between the In–ZnO:Ga MWs prepared with Au quasiparticle nanofilm decoration (Au@ZnO:Ga). It is also quite clear that the introduction of metal quasiparticle nanofilm decoration can also be employed to enhance the electric conduction, as demonstrated in Fig. 2(a) (red solid line). By applying bias on the bare ZnO:Ga MW, EL emission characteristics showed that green-lighting can be observed, with the emission peak centered around 509 nm, as exhibited in Fig. 2(b). Upon introducing Au quasiparticle nanofilm deposition, red-lighting can be obtained, with the lighting peak redshifted to be around 613 nm, as demonstrated in Fig. 2(c).

Interestingly, it has been reported that the Au quasiparticle nanofilms deposited on the ZnO:Ga MW can be transferred into physically isolated Au nanoparticles in the lighting region.[33,34] To exploit the modulation of Au nanoparticles on the lighting behavior of the single ZnO:Ga MW based incandescent-type emitter, Au quasiparticle nanofilms with sputtering times ranging from 30 to 80 s were also deposited onto sapphire substrates. After annealing in an Ar atmosphere at 500 °C, the size of the Au nanoparticles deposited on the sapphire substrate corresponded approximately to the Au nanoparticles, which localized at the emitting area of the single Au@ZnO:Ga MW based incandescent-type light source. Additionally, the absorption spectra for Au
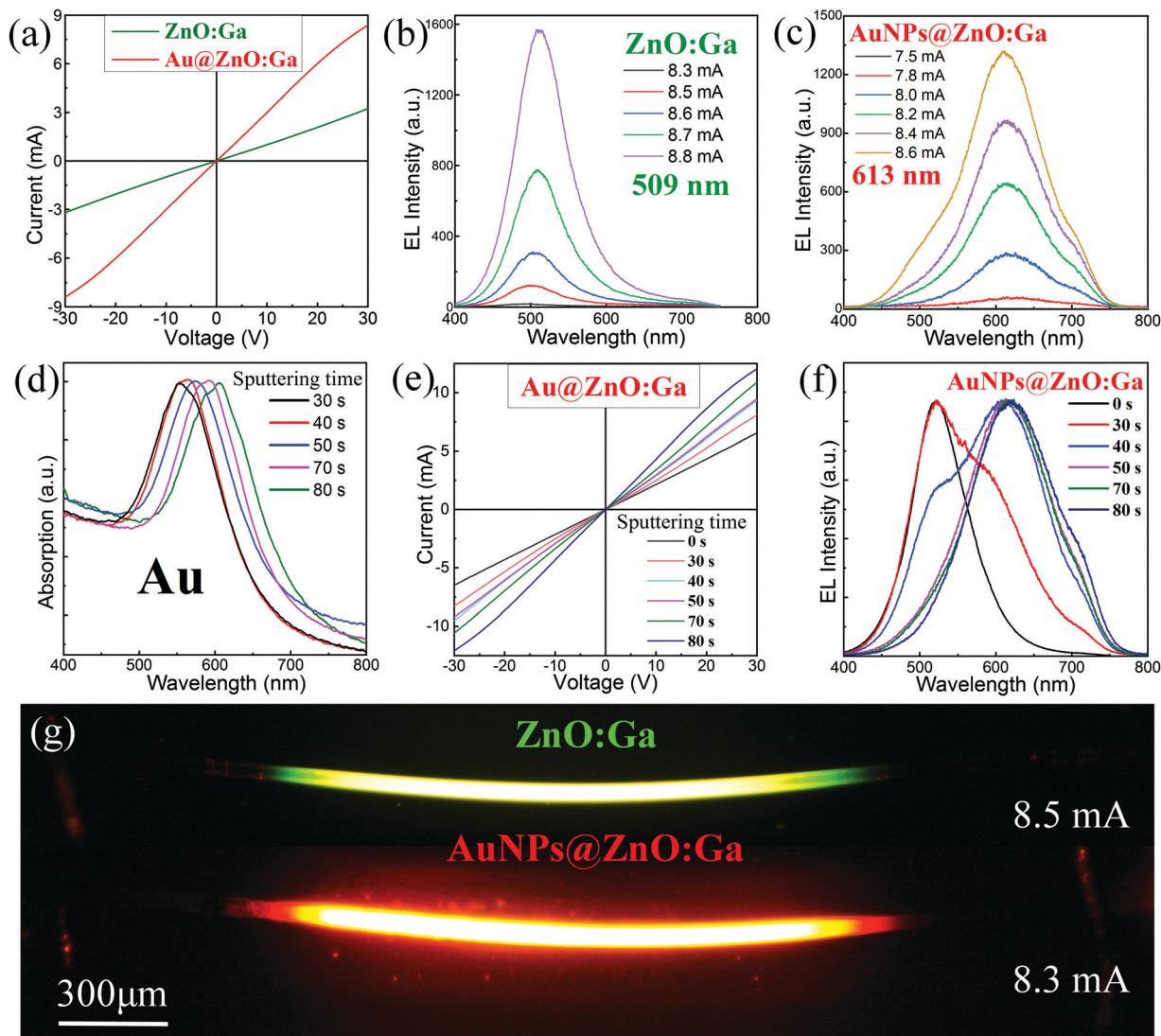
This journal is © The Royal Society of Chemistry 2019

J. Mater. Chem. C, 2019, **7**, 10933–10944 | **10935**

Fig. 2 (a) $I-V$ characteristics for single ZnO:Ga MW prepared with and without Au quasiparticle decoration (sputtering time: 60 s). (b) EL emission from single ZnO:Ga MW based fluorescent light source. (c) EL emission from single Au@ZnO:Ga MW based fluorescent light source (sputtering time: 60 s). (d) Normalized absorption spectra of Au nanoparticles deposited on the sapphire substrate with sputtering times ranging from 30 to 80 s (corresponding annealing temperature: 500 °C). (e) $I-V$ characteristics curves of single ZnO:Ga MW, as well as covered with Au quasiparticle nanofilm with the sputtering time ranging from 30 to 80 s. (f) Normalized EL spectra of single ZnO:Ga MW based fluorescent light source, and single Au@ZnO:Ga MW based emitter, with the sputtering time ranging from 30 to 80 s. (g) Optical microscope photographs of the bright and visible emission recorded from electrically driven single ZnO:Ga MW based incandescent-type emitter, and single Au@ZnO:Ga MW based incandescent-type emitter.

nanoparticles were measured, as displayed in Fig. 2(d). By increasing the sputtering time, redshift of the plasmonic absorption in the visible spectral region can be captured (550–605 nm).[21,37] To exploit the influence of the deposited Au quasiparticle nanofilm on the EL emission characteristics, fluorescent-type emitters consisting of single ZnO:Ga MWs decorated with Au quasiparticle nanofilm, with the sputtering times ranging from 30 s to 80 s, were also fabricated. Fig. 2(e) demonstrates the $I-V$ curves of the single ZnO:Ga MWs prepared without and with Au quasiparticle film deposition with the sputtering time ranging from 30 to 80 s. Obviously, increasing the sputtering time can lead to remarkable enhancement of the electronic transport properties.

By contrast, EL emission characteristics from the single ZnO:Ga MW based incandescent-type light source indicated that the dominant emission peaks centered at 520 nm, as demonstrated in Fig. 2(f). Following sputtering of the Au quasiparticle nanofilm (taking the sputtering time of 30 s for example), bimodal emissions with dominating lighting peaks centered approximately around 520 nm and 620 nm respectively, can be observed. Continuing to increase the injection current, the dominant emission wavelengths gradually blueshifted, and then finally centered around 520 nm. Upon increasing the sputtering time to 50 s, the emission wavelengths displayed a red-shift, and then finally centered at 625 nm. When the sputtering times increased to 80 s, the dominant

10936 | J. Mater. Chem. C, 2019, 7, 10933–10944

This journal is © The Royal Society of Chemistry 2019

emission peaks centered at 630 nm can be achieved (see Fig. 2(f)). Clearly, by adjusting the sputtering time, wavelength-tunable emissions from single Au@ZnO:Ga MW based incandescent-type light sources can be realized, with the dominating peaks tuned from 600 to 630 nm. Interestingly, when the sputtering time was ≤30 s, the thickness of the Au quasiparticle film is too thin and that may be evaporated and disappear by applying bias onto both ends of the wire; thus, the dominant emission wavelengths were firstly centered around 600 nm, and then blueshifted to be around 500 nm. However, once the sputtering time exceeded 120 s, the increasing size of Au nanoparticles will become less and less, leading to little redshift of the dominant emission wavelengths. In addition, when the sputtering time exceeded a certain value, such as 180 s, the single Au@ZnO:Ga MW can serve as the channel for electrical currents. Comparatively, by means of adjusting the sputtering times, the modulation of the emission features for the single ZnO:Ga MW based incandescent-type light source is still limited. The bright and visible emissions can also be directly recorded using optical microscopic CCD on account of the single ZnO:Ga MW based emitter, as well as the single Au@ZnO:Ga MW based emitter, as shown in Fig. 2(g).

Taking the sputtering time ~60 s for instance, the dominant emission wavelengths from the single Au@ZnO:Ga MW based filament-type emitter centered around 600 nm, which cannot be matched with the absorption peak of the Au nanoparticles (~550 nm). Meanwhile, PL measurements also demonstrated

that NBE-type emission dominated the emission spectrum from the single Au@ZnO:Ga MW in the ultraviolet spectral band, together with negligible visible emission. Therefore, the effect of the Au quasiparticle nanofilms on the EL emission characteristics of the single ZnO:Ga MW based fluorescent-type emitter cannot be attributed to selective amplification and enhancement of the Au-plasmon induced near field coupling and enhancement.[7,21,28,38,39] Additionally, when the deposited Au quasiparticle film was thin enough, the transfer from red lighting into green lighting with increasing injection current can also rule out the contribution that Au-related deep levels could be formed in the band-gap structure of ZnO:Ga. Besides, another fluorescent emitter composed of a single Au@ZnO:Ga MW was also constructed (sputtering time: 60 s). Bright and red emission can be collected when the injection current exceeded a certain value, as shown in Fig. 3(a). Furthermore, with continuous increase of the injection current, instantaneous electrical breakdown can happen, with the broken region located towards the hottest spot, which is consistent with the brightest region, as shown in Fig. 3(b) and (c).[40] Instantaneous electrical breakdown of the single ZnO:Ga MW was also carried out, as indicated in Fig. S5 in the ESI.† To characterize the Joule heating effect on the surface morphology of the Au nanostructures, it was found that Au still remained as the quasiparticle nanofilm in the non-lighting regions (I-region), as displayed in Fig. 3(d) and (e). In the critical region between non-lighting and
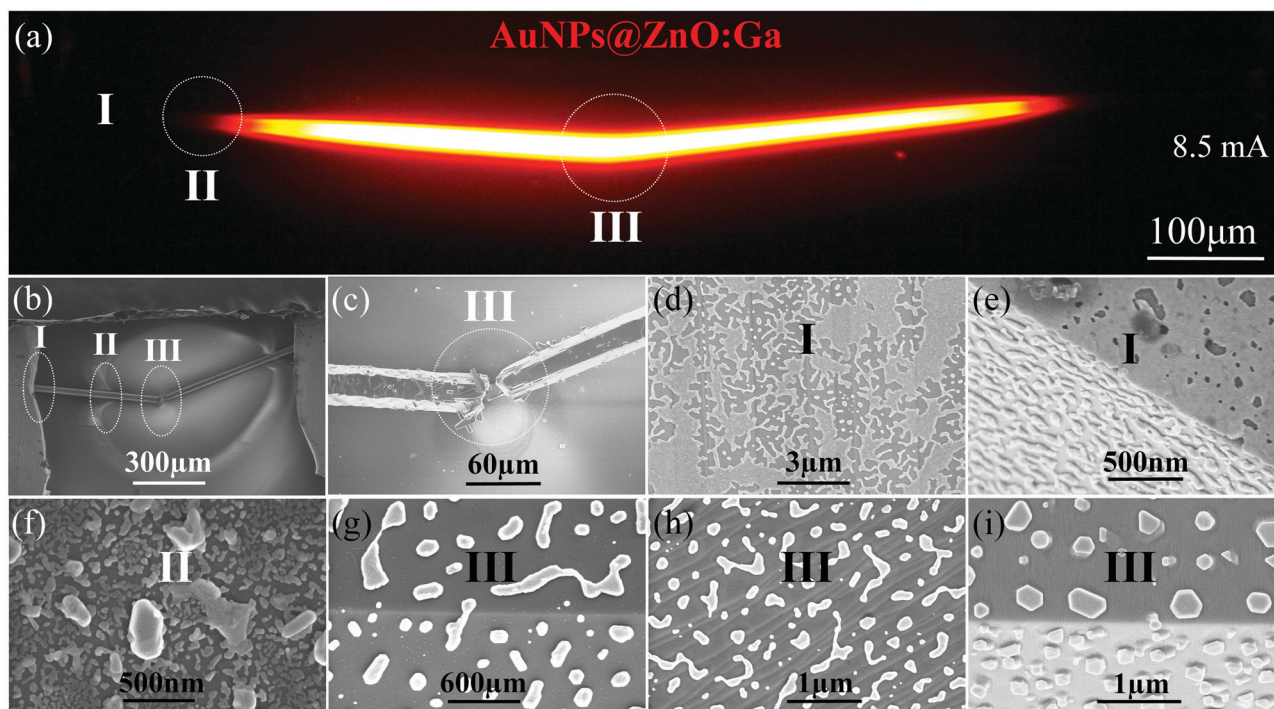

Fig. 3 (a) Bright and red emissions from electrically driven single Au@ZnO:Ga MW based filament-type light source (sputtering time: 60 s), with three different regions marked: I denoting the non-lighting region, II denoting the critical region between lighting and non-lighting, and III denoting the lighting region located towards the brightest spot, respectively. (b) SEM image of single Au@ZnO:Ga MW based filament-type light source, with the instantaneous electrical breakdown located towards the center of the wire. (c) Amplified SEM image of the instantaneous electrical breakdown region. SEM images of Au quasiparticle nanofilm located in the I-region (d) and (e). SEM images of Au nanostructures located in the II-region ranging from the non-lighting region to lighting region (f)–(h), respectively. (i) SEM image of physically isolated Au nanoparticles located in the III-region.

lighting, a transition from quasiparticle nanofilm into isolated Au nanoparticles can occur, as demonstrated in Fig. 3(f)–(h) respectively in the III-region. Further to illustrate the physical procedure of physically isolated Au nanoparticles transferred from the quasiparticle nanofilm, which were located in the lighting region, another single Au@ZnO:Ga MW based fluorescent-type light source was also prepared. Detailed information on the optical microscope photographs of the bright and visible emission, EL emission spectra, as well as SEM images of the Au nano-structures deposited on the ZnO:Ga MW were also captured, as indicated in Fig. S6 and S7 in the ESI.† Therefore, a typical incandescent light source composed of physically isolated Au nanoparticles decorated on a single ZnO:Ga MW (AuNPs@ZnO:Ga) can be fabricated.

To identify the relationship between metal plasmons of Au nanoparticles and the emission behaviors from the single Au@ZnO:Ga MW based filament-type light source with the sputtering time ranging from 30 to 80 s, surface morphologies of Au nanostructures located in the emission regions were also characterized (see Fig. S8 in the ESI†). Thereby, increasing the sputtering time can lead to enlarging the size of the self-annealing induced Au nanoparticles, as well as an increased concentration of the Au nanoparticles aggregation. In contrast, Au quasiparticle nanofilms were also deposited on the sapphire substrate, and then subsequently annealed at 500 °C. The experimental finding demonstrated that the Au quasiparticles nanofilm can be annealed into isolated Au nanoparticles, with the sizes being approximate to the EL emission induced by the formation of Au nanoparticles, which are located in the lighting region of the wire. Consequently, the Joule heating effect induced the generation of temperature which could be estimated to be around 500 °C roughly.[12,33,41]

Specially, it is also worth pointing out that Au quasiparticle films localized towards the III-region can be transformed into the isolated Au nanoparticles; thus, a resistive heating effect can function as a crucial character in the working principle of the EL emission.[24,40,41] As previously mentioned, the applied bias can be considered as being directly applied to the emission zone, leading to the formation of strong and modest electric fields ($\sim 10^6$ V m^{-1}).[12,32,33,41] To provide a visual picture for Au-plasmon mediated modulation of the EL emission features of the single ZnO:Ga MW based filament-type emitter, a simple mechanism diagram can be depicted, details can be seen Fig. S9 in the ESI.† With the aid of metal quasiparticle film decoration, electronic transport properties of the as-synthesized MW can greatly be enhanced. Due to the poor thermal conductance of the highly-crystallized ZnO:Ga MWs, the heat dissipation is greatly suppressed along the axial direction. Thereby, the hottest spot can be formed towards the center of the MW, resulting in an adequate electric field. The electrons transported in the MW-channel can be accelerated to become energetic electrons.[24,33,41]

Meanwhile, the deposited quasiparticle films located towards the hottest regions would be annealed into random isolated Au nanoparticles due to self-annealing effects. Therefore, plasmons in Au nanoparticles could be excited by means of inelastic impact ionization with energized electrons, being transported in the MW-channel. After relaxation, metal plasmons can decay nonradiatively, and then transfer the energy into excited electrons. Thus, a non-thermal equilibrium distribution of hot electrons can be created, which is located well above the Fermi-level of the neighboring ZnO:Ga.[28,42] Once possessing adequate energies well above the Schottky barrier at the metal–semiconductor interface, the energized electrons can be directly injected into the conduction band of the adjacent ZnO:Ga. Meanwhile, there is an exponentially decreased probability of the energized electrons possessing energy lower than the Schottky barrier, which could be tunneled, thus contributing to enhanced electronic transmission capacities, which is in accordance with the observed experimental results.[38,42,43] By increasing the injection current, one can achieve rapid acceleration of hot electrons. After thermalized relaxation, a population distribution of non-equilibrium hot electrons can be created in the energy-level configuration of the adjacent ZnO:Ga, leading to a broad and inhomogeneous energy profile for the non-equilibrium electrons.[38,42] Following on, radiative recombination can occur, thus leading to modification of the EL emission characteristics from the single ZnO:Ga MW based filament-type light source. Therefore, due to the versatility of the metal nanostructures with tunable plasmonic plasmons, the hybrid architecture composed of a single ZnO:Ga MW prepared with metal nano-structures evaporation can offer a potential candidate to construct low-dimensional wavelength-tunable emission devices in an ultrawide spectral band.[18,24,33]

3.3 Electrical-injection spasing action from cross-stacked architecture composed of single ZnO:Ga MW, crossed with another AuNPs@ZnO:Ga MW

One-dimensional (1D) micro/nanostructures, being treated as building blocks, have been widely utilized to construct versatile, multifunctional and universalizable optoelectronic devices, such as single-photon sources, photodetectors, solar cells, etc. The fascinating structures of such cross-stacked architecture arrays have afforded generic possibilities for the construction of integrated optoelectronic devices, accompanied with addressable functions located at each crossed point.[1,3–6] By means of the availability of well-defined ZnO:Ga MWs, a cross-stacked architecture composed of a single ZnO:Ga MW, crossed with another ZnO:Ga MW prepared with Au nanoparticles deposition (AuNPs@ZnO:Ga) was fabricated, as indicated in Fig. S10 in the ESI.† The single bare ZnO:Ga MW was selected to construct a green-lighting fluorescent emitter, as shown in Fig. 4(a). While, the other AuNPs@ZnO:Ga MW can be utilized to achieve red-emission, as demonstrated in Fig. 4(b). Due to the lighting areas being localized towards the center of the MWs, two kinds of hybrid architectures were established: emission regions separated from each other, and emissions regions overlapped with each other. For comparison, hybrid architectures with the emission regions separated from each other were characterized, detailed information on the emission features can be found in Fig. S11 in the ESI.† By applying bias on A–C and B–D respectively, the emitted photons were recorded, with the emission spectra shown in Fig. S12 in the ESI.†

10938 | J. Mater. Chem. C, 2019, 7, 10933–10944

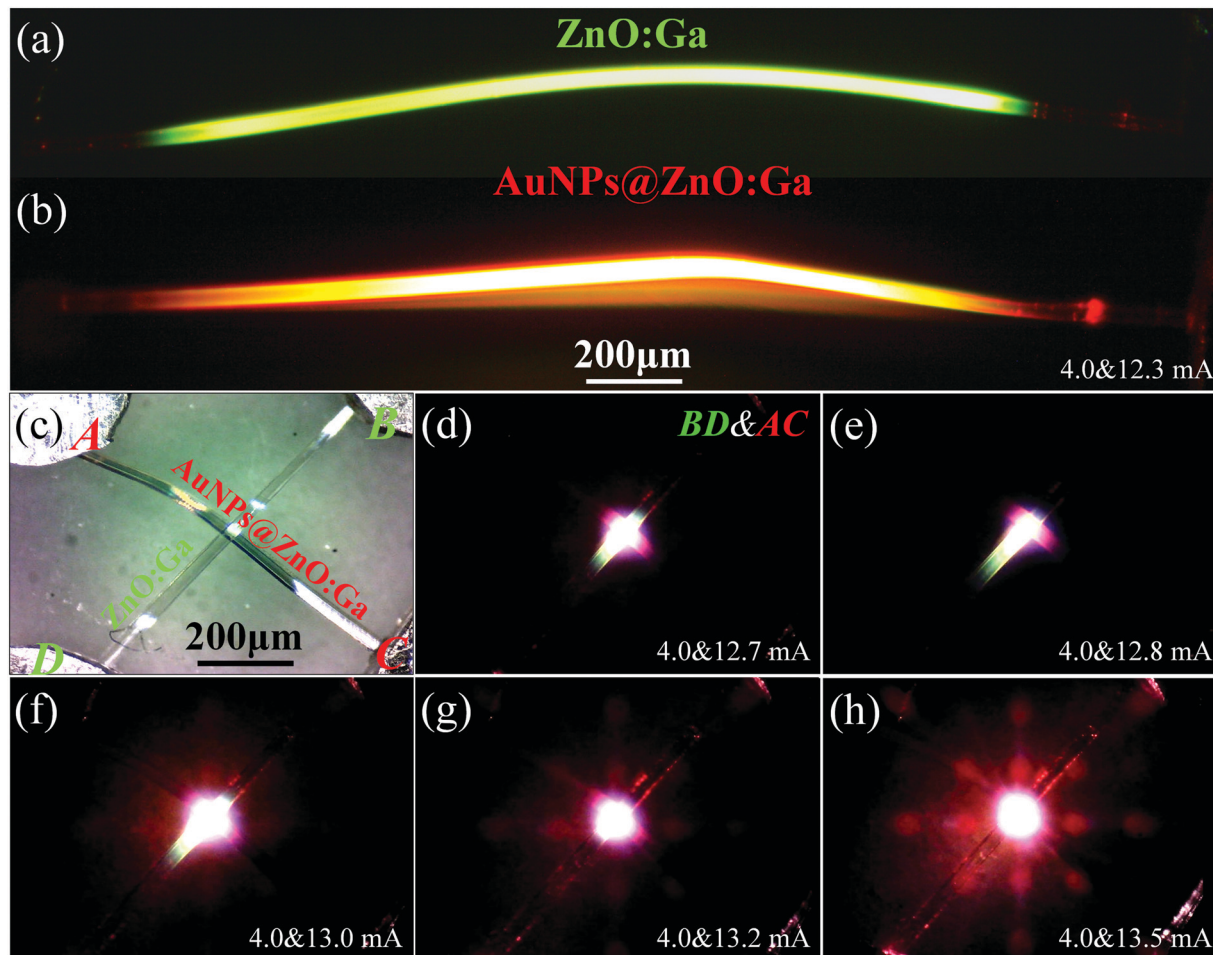This journal is © The Royal Society of Chemistry 2019

Fig. 4 Optical microscope images from cross-stacked architecture composed of single ZnO:Ga MW, crossed with another AuNPs@ZnO:Ga MW: (a) optical microscope image of bright and green emission from single ZnO:Ga MW based filament-type light source. (b) Optical microscope image of bright and red emission from single AuNPs@ZnO:Ga MW based filament-type light source. (c) Typical optical microscope images of lighting from the cross-stacked architecture. The injection current for the bare MW was maintained at 4.0 mA, while increasing the injection current of the other AuNPs@ZnO:Ga MW ranging from (d) 12.7 mA; (e) 12.8 mA; (f) 13.0 mA; (g) 13.2 mA; and finally to (h) 13.5 mA.

As mentioned above, the cross-stacked architecture comprising a single ZnO:Ga MW, crossed with the other AuNPs@ZnO:Ga MW was fabricated. The In electrodes, denoted as A, B, C and D respectively, were fixed on the ends of the crossed MWs, as demonstrated in Fig. 4(c). By applying bias onto the electrodes A and D, green light-emission can be observed, with the emission regions located towards the segment of the single ZnO:Ga MW. The typical optical microscope images were captured, and are displayed in Fig. S13 in the ESI.† When applying the bias simultaneously onto the crossed MWs, such as A–C, B–D, for instance, and maintaining the injection current for the bare ZnO:Ga MW at a stable value (B–D), such as 4.0 mA, while increasing the injection current for the other MW (A–C) ranging from 12.0 to 13.5 mA, bright and localized emissions can be observed, with the emission regions localized at the crossed regions. The brightness and light emission regions increase with the injection current for the single AuNPs@ZnO:Ga MW. The brightest spot for the light-emitting behavior is always localized at the crossed

region of the cross-stacked architecture, with the corresponding optical microscope images for the visible emission shown in Fig. 4(d)–(f). The light-emitting is intense enough to be seen by the naked eye. Specifically, when the injection current exceeded 13.0 mA, the lighting regions reduced to the crossed zone, as shown in Fig. 4(g) and (h).

The electronic transport properties of the crossed MWs were characterized, with the bias applied onto the electrodes, such as A–C, B–D, and B–C, respectively, as demonstrated in Fig. 5(a). The I–V characteristic curves of the single ZnO:Ga MW (green solid line), and the other AuNPs@ZnO:Ga MW (red solid line) respectively, revealed linear and symmetric shapes, indicating the ohmic contact forming between the In and the MWs (Fig. 5b). Although both the emission regions crossed with each other, the underlying trends for the separated MWs were relatively impervious. When applying the bias onto the electrodes B–C, the I–V curve exhibited a nonlinear tendency being analogous to the symmetrical quasi-Schottky junction formed between the AuNPs@ZnO:Ga MW and the other
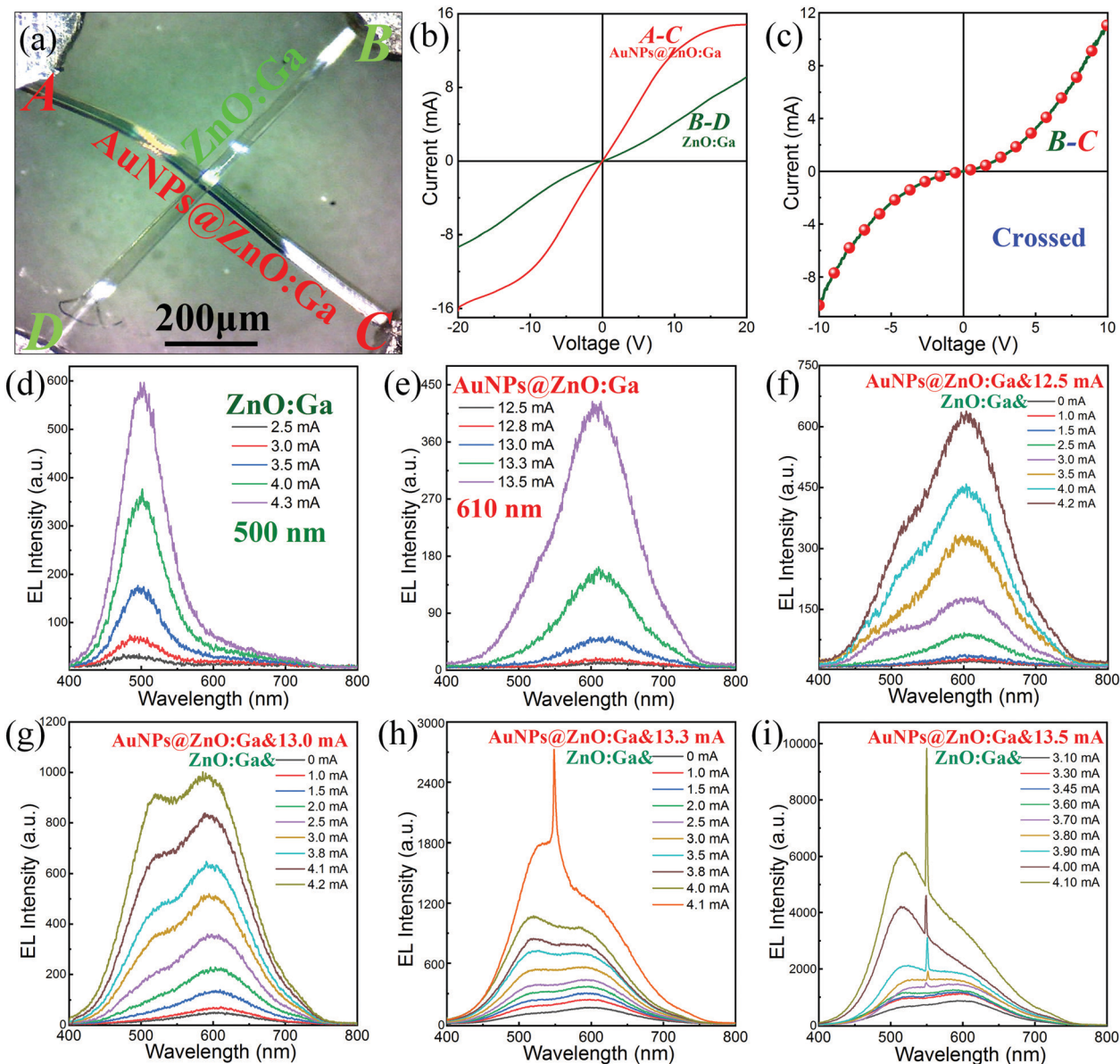
This journal is © The Royal Society of Chemistry 2019

J. Mater. Chem. C, 2019, 7, 10933–10944 | 10939

Fig. 5 EL emission characteristics from the cross-stacked architecture: (a) optical microscope image of the cross-stacked architecture. (b) *I−V* characteristics curves of the single ZnO:Ga MW (B−D), and the other AuNPs@ZnO:Ga MW (A−C) respectively. (c) *I−V* behavior of the crossed MWs (B−C). (d) EL emission spectra from the single ZnO:Ga MW based filament-type emitter. (e) EL emission spectra from the other AuNPs@ZnO:Ga MW based filament-type emitter. The emitted photons were also collected with the bias applied onto both the crossed MWs simultaneously, for instance, the injection current for the ZnO:Ga MW ranging from 0 to 4.2 mA, while maintaining the injection current for the AuNPs@ZnO:Ga MW at a fixed value, such as (f) 12.5 mA; (g) 13.0 mA. When the injection current of the AuNPs@ZnO:Ga MW increased to be 13.3 mA (h), a sharp peak centered at 550 nm appeared on the emission spectrum, accompanied by a rapid narrowing of the FWHM to be 2 nm; when the injection current of the AuNPs@ZnO:Ga MW increased to be 13.5 mA (i), sharp emission peaks centered at 550 nm can also be captured, accompanied by the appearance of a FWHM of 2 nm.

ZnO:Ga MW, as displayed in Fig. 5(c). This may be due to the sandwiched Au nanoparticles, where a significant tunneling barrier between the crossed MWs could be formed.[27,38,44] To investigate the localized light emissions from the crossed MWs, the emission spectra were also collected. Firstly, when the bias was applied onto the single bare ZnO:Ga MW without any operation on the other AuNPs@ZnO:Ga MW, bright and green lighting can be recorded from the single ZnO:Ga MW based fluorescent emitter, with the emission peaks centered around 500 nm, as indicated in Fig. 5(d). Similarly, when we

also applied bias onto the other AuNPs@ZnO:Ga MW, bright and red emission was acquired, with the dominating emission peaks centered around 610 nm, as indicated in Fig. 5(e).

When the bias was applied onto both the crossed MWs simultaneously, for instance, the injected current of the AuNPs@ZnO:Ga MW was maintained at a fixed value, such as 12.5 mA, while increasing the injection current of the single ZnO:Ga MW gradually, Fig. 5(f) demonstrates that the dominating emission peaks were centered around 605 nm. Upon increasing the injection current of the AuNPs@ZnO:Ga MW to 13.0 mA, the

dominating emission wavelengths for the crossed MWs were first found to be centered around 600 nm, then transferred into bimodal-emission, with the emission peaks centered at 520 nm and 600 nm, respectively (see Fig. 5(g)). With a further increase in the injection current of the AuNPs@ZnO:Ga MW to 13.3 mA, the emission wavelengths for the crossed architecture were found to be firstly centered around 600 nm, and then transferred into dual-emission, with corresponding emission peaks centered at 520 nm and 600 nm, respectively. Especially, when the injection current for the single ZnO:Ga MW exceeded 4.1 mA, a sharp emission peak from the crossed MWs can be recorded, with the prominent emission peak centered at 550 nm accompanied by a FWHM that narrowed to 2 nm, as shown in Fig. 5(h). Finally, when the injection current of the AuNPs@ZnO:Ga MW increased to 13.5 mA, the dominant emission peaks for the crossed architecture were found to be first centered at 600 nm, and then transferred into dual-emission, with dominating emission peaks centered around 520 nm and 600 nm, respectively. Once the injection current for the bare ZnO:Ga MW exceeded 3.70 mA, a sequence of sharp emissions can also be observed, with the dominating emission-peak centered at 550 nm accompanied by a rapid narrowing of the FWHM to 2 nm, as shown in Fig. 5(i).

To explore the sharp emission features, a comparison of the emission spectra of single ZnO:Ga MW and single AuNPs@ZnO:Ga MW based filament-type emitters, the sharp emission spectrum from the crossed MWs, and the absorption spectrum of Au nanoparticles were taken into account, as indicated in Fig. 6(a). By contrast, the sharp emission peak centered at 550 nm cannot be derived from the single bare ZnO:Ga MW, or the single AuNPs@ZnO:Ga MW based filament-type emitters. It also cannot be attributed to the summation of the emissions from the crossed MWs. In particular, it can be acknowledged that the dominating emission peak is consistent with the absorption peak of the Au nanoparticles, which are located in the sandwiched regions of the crossed MWs. Therefore, the sharp emission may be ascribed to the Au-nanoparticle plasmons amplification, which is confined in the cross-stacked region.[1,45,46] Especially, the integrated emission intensity for the cross-stacked architecture was calculated as a function of the injection current for the single ZnO:Ga MW ranging from 2.5 to 4.1 mA, while maintaining the injection current of the other AuNPs@ZnO:Ga MW at 13.5 mA. Fig. 6(b) demonstrated a typical nonlinear relationship. Therefore, the output lighting displayed a distinct turning point at the threshold current of 3.9 mA. When the injection current of the bare MW reached 3.9 mA, a sharp peak can be observed over the spontaneous emission background, accompanied with the spectral linewidth rapidly narrowing to be 2 nm, suggesting the occurrence of amplified spontaneous emission. With a further increase in the injection current beyond 3.90 mA, the EL spectra are dominated by sharp emission peaks, which centered at 550 nm, accompanied by an FWHM of 2 nm. In addition, the dependence of the spectral linewidth on the injection current of the single AuNPs@ZnO:Ga MW was also investigated. The experimental data revealed that an abrupt decrease in the FWHM narrowing from 60.0 to 2.0 nm can occur by increasing the injection current ranging from 3.0 to 4.1 mA

(see Fig. 6(b)). Therefore, electrical-pumping spasing action could be achieved on the basis of the cross-stacked architectures.[39,45,46]

Fig. 6(c) illustrates the SEM image of the crossed MWs, with isolated Au nanoparticles sandwiched into the crossed region. Additionally, SEM images of the single ZnO:Ga MW, crossed with the other AuNPs@ZnO:Ga MW, together with the amplified SEM image of the crossed MWs, can also be seen in Fig. S14 in the ESI.† Physically isolated Au nanoparticles were sandwiched into the crossed regions, which is in accordance with the localized emission regions. With well-defined facets, atomically smooth interfaces and a contact geometry for the as-synthesized hexagonal ZnO:Ga MWs, a hybrid plasmonic nanocavity composed of a ZnO:Ga–AuNPs–ZnO:Ga based sandwich structure could be formed.[47–50] This may be treated as the precursor to achieve strong localization of the lighting-emission. To examine the potential working principle of the cross-stacked architecture, a schematic diagram of the hybrid plasmonic Fabry–Perot (F–P) nanocavity composed of the ZnO:Ga–AuNP–ZnO:Ga based sandwich structure was constructed, as shown in Fig. 6(d). The crossed MWs can support a plasmonic mode, with corresponding electric field intensity strongly confined within the gap between the crossed MWs. The highly smooth surfaces of the MWs can serve as high quality optical mirrors, which stand perpendicular to the axial direction, leading to the construction of an F–P mode optical cavity. The corresponding nanocavity length, L_c, was determined by the size of the sandwiched Au nanoparticles. Therefore, the sharp emissions from the crossed MWs may be derived from the hybrid plasmonic F–P mode optical nanocavity. The electrical-pumping spasing features, such as the sharp emission peak, spectral linewidth, and threshold current, may be dependent on the sizes of the Au nanoparticles, and optical and electrical properties of the as-synthesized ZnO:Ga MWs.[23,48,49]

To illustrate that the cross-stacked architecture can afford a potential candidate to achieve electrical-injection spasing action at nanometer-scale dimensions, the electronic transport properties of the crossed MWs were taken into account. Due to the large differential electrical conductance of the crossed MWs (the single ZnO:Ga MW can be treated as a semiconducting MW, while the other AuNPs@ZnO:Ga MW should be treated as a quasi-metallic MW), as well as the gap at the nanometer-level (the diameter of the Au nanoparticles is ∼100 nm), hot electrons could be tunneled, accompanied with the electronic transport process from the Au@ZnO:Ga MW to the bare ZnO:Ga MW. This finding can also be corroborated by the quasi-Schottky potential barrier, which was mentioned above. Thus, when the bias applied onto the crossed MWs is large enough, hottest spots localized towards the crossed regions could be formed. Then, the modest and adequate electric field can also be produced, with energized electrons being accelerated towards the emission regions of the Au@ZnO:Ga MWs, and then becoming spatially localized towards the crossed regions. Afterwards, localized surface plasmons generated from the sandwiched Au nanoparticles can be stimulated through inelastic collision ionization with tunneling energetic
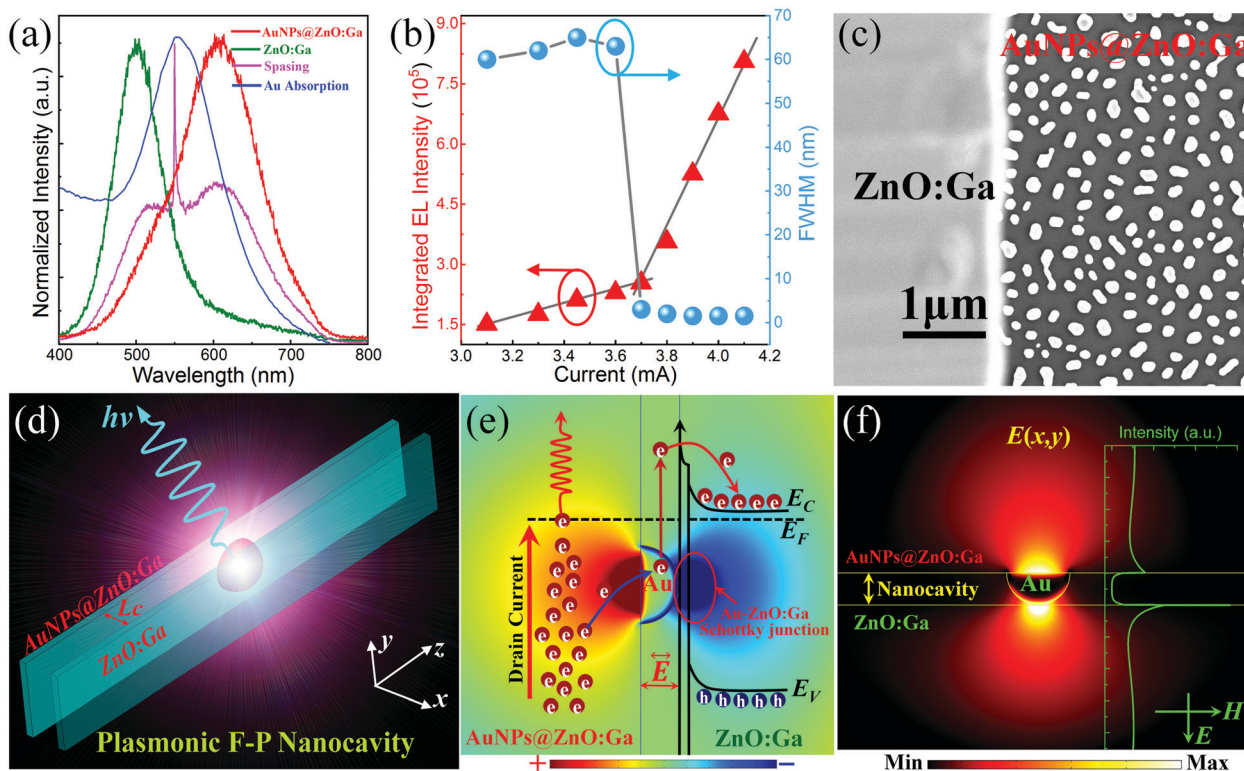
This journal is © The Royal Society of Chemistry 2019

J. Mater. Chem. C, 2019, 7, 10933–10944 | 10941

Fig. 6 Au-plasmon amplified EL emission from the cross-stacked architecture: (a) comparison of the emission spectra from single ZnO:Ga MW and single AuNPs@ZnO:Ga MW based filament-type emitters, absorption of Au nanoparticles, and the sharp emission spectrum from the crossed MWs. (b) Integrated emission intensities for the cross-stacked architecture *versus* the injection current of the single ZnO:Ga MW, while maintaining the injection current of the AuNPs@ZnO:Ga MW at 13.5 mA; also, the FWHM of the crossed MWs *versus* the injection current of the bare ZnO:Ga MW, while maintaining the injection current of the AuNPs@ZnO:Ga MW at 13.5 mA. (c) SEM images of the crossed MWs, with Au nanoparticles sandwiched in the crossed regions. (d) Diagrammatic drawing of the hybrid plasmonic nanocavity composed of a single ZnO:Ga MW, crossed with a AuNPs@ZnO:Ga MW. (e) When applying bias onto both the crossed MWs simultaneously, an electrical potential field difference $\vec{E}$ between the crossed region can be formed. Thus, by increasing the applied bias, one can facilitate electrons tunneling from the AuNPs@ZnO:Ga into the ZnO:Ga MW-channel. (f) The formation of the hybrid plasmonic nanocavity, in which Au plasmons induced a significant enhancement of the electric field $E(x,y)$. The inset shows the absorption peak for the Au nanoparticles.

electrons. That is, under the adequate large electrical potential difference, hot electrons can migrate into the bare ZnO:Ga MWs through the Schottky barrier, as displayed in Fig. 6(e).[28,29,38,42,46]

In particular, increasing applied bias can be utilized to amplify plasmonic energies, facilitating the tunneling of electrons from the AuNPs@ZnO:Ga MW into the bare ZnO:Ga MW-channel with the aid of the sandwiched Au nanoparticles. When the electric potential difference between the crossed MWs was sufficiently large enough, localized surface plasmon resonances of the Au nanoparticles can be motivated in the crossed regions, leading to significant enhancement of the tunneling electrons, as shown in Fig. 6(f) (plasmons of Au nanoparticles, electric field distribution, together with hot-carrier distribution can be seen in Fig. S15 and S16 in the ESI†). Strong electric field confinement could be formed in the nanocavity between the plasmonic mode of the Au nanoparticles and nanocavity mode, which was produced by the crossed ZnO:Ga MWs. The extraordinary localization of the light-emitting regions towards the crossed regions of the cross-stacked architectures could be ascribed to strong plasmonic confinement, leading to an excellent spatial superposition

between the plasmons of the Au nanoparticles and the emitted photons of crossed MWs, which can enable the realization of the electrically pumped spasing action.[39,44,45,48]

In such cross-stacked architecture based light-emitting devices, three precursor conditions are critical to achieve electrically pumped spasing action: (1) light-emission can be achieved from electrically driven individual ZnO:Ga MWs based filament-type emitters, with the emissive regions localized towards the center of the wire. In particular, by introducing metal nanostructures decoration, such as Au nanoparticles, light-emitting characteristics can be modulated; (2) great differences in the electronic conductance between the crossed MWs should be a prerequisite. That is, during the fabrication of the cross-stacked architectures, the bare ZnO:Ga MW could be treated as a semiconducting wire, while the other AuNPs@ZnO:Ga MW should be treated as a quasi-metallic wire. (3) It is crucial that the emission regions from the crossed MWs should be overlapped with each other. Regrettably, further investigations are still needed, such as (i) by introducing metal nanostructures deposition, the effective modulation of the single ZnO:Ga MW based incandescent-type emitter should

10942 | *J. Mater. Chem. C*, 2019, 7, 10933–10944

This journal is © The Royal Society of Chemistry 2019

be further investigated; (ii) electrical-pumping spasing can be achieved on account of the hybrid plasmonic F–P mode nano-cavity, nevertheless, the spasing stability and output mode, especially the single mode spasing feature remained mysterious; (iii) the dominating lasing wavelength relied on the absorption peak of the sandwiched Au-nanoparticles, nevertheless, the modu-lation of the size of the Au nanoparticles was still restricted.

4 Conclusion

In summary, tunneling diodes were constructed based on a cross-stacked architecture, which was composed of a single ZnO:Ga MW, crossed with another AuNPs@ZnO:Ga MW. The cross-stacked architecture demonstrated a well-defined Schottky junction feature when both the emission regions overlapped with each other. By applying bias onto the crossed MWs simultaneously, localized and bright light-emission at the crossed region can be observed, with the emission regions experiencing a process that enlarged at first, and then reduced to the crossed regions sharply. Meanwhile, a sharp emission peak centered at 550 nm, with the spectral linewidth narrowing to 2 nm emerged in the emission spectra. Analysis of the tunneling electrons and light emission feature illustrated that Au-plasmons dominated the sharp EL emission for the lighting localization and amplification. We believe that the realization of electrically pumped spasing action and tunneling diodes using cross-stacked MWs covered with metal nanostructures opens up a simple and scalable route towards low-cost fabrica-tion of highly integrated microscale/nanoscale light-emitting devices, such as electrical spasers, metal plasmons induced tunneling diodes and so on.

Conflicts of interest

There are no conflicts to declare.

Acknowledgements

References

1 D. Wang, W. Wang, M. P. Knudson, G. C. Schatz and T. W. Odom, *Chem. Rev.*, 2018, **118**, 2865–2881.

2 J. W. Liang, I. Kaminer, O. Ilic, J. D. Joannopoulos and M. Soljacic, *Nat. Photonics*, 2015, **10**, 46–52.

3 D. Liang, X. Huang, G. Kurczveil, M. Fiorentino and R. G. Beausoleil, *Nat. Photonics*, 2016, **10**, 719–722.

4 Z. Zhou, B. Yin and J. Michel, *Light: Sci. Appl.*, 2015, **4**, e358.

5 Y. H. Ting, J. Y. Chen, C. W. Huang, T. K. Huang, C. Y. Hsieh and W. W. Wu, *Small*, 2018, **14**, 1703153.

6 Z. Zhang, K. Guo, Y. Li, X. Li, G. Guan, H. Li, Y. Luo, F. Zhao, Q. Zhang and B. Wei, *Nat. Photonics*, 2015, **9**, 233–238.

7 D. Wang, M. R. Bourgeois, W.-K. Lee, R. Li, D. Trivedi, M. P. Knudson, W. Wang and G. C. Schatz, *Nano Lett.*, 2018, **18**, 4549–4555.

8 Y. H. Ra, R. Wang, S. Y. Woo, M. Djavid, S. M. Sadaf, J. Lee, G. A. Botton and Z. Mi, *Nano Lett.*, 2016, **16**, 4608–4615.

9 S. Krotkus, D. Kasemann, S. Lenk, K. Leo and S. Reineke, *Light: Sci. Appl.*, 2016, **5**, e16121.

10 Y. Huang, X. Duan and C. M. Lieber, *Small*, 2005, **1**, 142–147.

11 Y. Li, F. Qian, J. Xiang and C. M. Lieber, *Mater. Today*, 2006, **9**, 18–27.

12 M. Jiang, G. He, H. Chen, Z. Zhang, L. Zheng, C. Shan, D. Shen and X. Fang, *Small*, 2017, **13**, 1604034.

13 L. Yang, M. Jiang, G. He, S. Li, Z. Zhang, B. Li, H. Zhao, C. Shan and D. Z. Shen, *ACS Appl. Mater. Interfaces*, 2017, **9**, 40743–40751.

14 X. Zhang, L. Li, J. Su, Y. Wang, Y. Shi, X. Ren, N. Liu, A. Zhang, J. Zhou and Y. Gao, *Laser Photonics Rev.*, 2014, **8**, 429–435.

15 Z. Yang, D. Wang, M. Chao, Z. Wu, W. Yong, Y. Ma, D. Lun, X. Liu, T. Hasan and L. Xu, *Nano Lett.*, 2014, **14**, 3153–3159.

16 W. K. Hong, J. I. Sohn, D. K. Hwang, S. S. Kwon, G. Jo, S. Song, S. M. Kim, H. J. Ko, S. J. Park and M. E. Welland, *Nano Lett.*, 2008, **8**, 950–956.

17 G. D. Yuan, W. J. Zhang, J. S. Jie, X. Fan, J. X. Tang, I. Shafiq, Z. Z. Ye, C. S. Lee and S. T. Lee, *Adv. Mater.*, 2008, **20**, 168–173.

18 M. Zapf, R. Roder, K. Winkler, L. Kaden, J. Greil, M. Wille, M. Grundmann, R. Schmidt-Grund, A. Lugstein and C. Ronning, *Nano Lett.*, 2017, **17**, 6637–6643.

19 K. Ding and C. Z. Ning, *Light: Sci. Appl.*, 2012, **1**, e20.

20 W. Strek, B. Cichy, L. Radosinski, P. Gluchowski, L. Marciniak, M. Lukaszewicz and D. Hreniak, *Light: Sci. Appl.*, 2015, **4**, e237.

21 T. Klar, M. Perner, S. Grosse, G. V. Plessen, W. Spirkl and J. Feldmann, *Phys. Rev. Lett.*, 1998, **80**, 4249–4252.

22 K. H. Shokri, J. H. Yun, Y. Paik, J. Kim, W. Anderson and S. J. Kim, *Nano Lett.*, 2016, **16**, 250–254.

23 M. Buret, A. V. Uskov, J. Dellinger, N. Cazier, M. M. Mennemanteuil, J. Berthelot, I. V. Smetanin, I. E. Protsenko, G. Colas-Des-Francs and A. Bouhelier, *Nano Lett.*, 2015, **15**, 5811–5818.

24 P. Rai, N. Hartmann, J. Berthelot, J. Arocas, G. Colas des Francs, A. Hartschuh and A. Bouhelier, *Phys. Rev. Lett.*, 2013, **111**, 026804.

25 S. Eustis and M. A. El-Sayed, *Chem. Soc. Rev.*, 2006, **35**, 209–217.

26 A. Sobhani, M. W. Knight, Y. Wang, B. Zheng, N. S. King, L. V. Brown, Z. Fang, P. Nordlander and N. J. Halas, *Nat. Commun.*, 2013, **4**, 1643.

27 K. Wu, J. Chen, J. R. McBride and T. Lian, *Science*, 2015, **349**, 632.

This journal is © The Royal Society of Chemistry 2019

J. Mater. Chem. C, 2019, **7**, 10933–10944 | **10943**

28 A. Pescaglini, A. Martín, D. Cammi, G. Juska, C. Ronning, E. Pelucchi and D. Iacopino, *Nano Lett.*, 2014, **14**, 6202–6209.

29 C. Clavero, *Nat. Photonics*, 2014, **8**, 95–103.

30 G. Lozano, S. R. Rodriguez, M. A. Verschuuren and J. G. Rivas, *Light: Sci. Appl.*, 2016, **5**, e16080.

31 D. Wang, A. Yang, W. Wang, Y. Hua, R. D. Schaller, G. C. Schatz and T. W. Odom, *Nat. Nanotechnol.*, 2017, **12**, 889–894.

32 Y. Vardi, E. Cohen-Hoshen, G. Shalem and I. Bar-Joseph, *Nano Lett.*, 2016, **16**, 748–752.

33 Y. Liu, M. Jiang, Z. Zhang, B. Li, H. Zhao, C. Shan and D. Shen, *Nanoscale*, 2018, **10**, 5678–5688.

34 M. Jiang, W. Mao, X. Zhou, C. Kan and D. N. Shi, *ACS Appl. Mater. Interfaces*, 2019, **11**, 11800–11811.

35 G. H. He, M. M. Jiang, L. Dong, Z. Z. Zhang, B. H. Li, C. X. Shan and D. Z. Shen, *J. Mater. Chem. C*, 2017, **5**, 2542–2551.

36 N. Han, F. Wang, J. J. Hou, S. P. Yip, H. Lin, F. Xiu, M. Fang, Z. Yang, X. Shi and G. Dong, *Adv. Mater.*, 2013, **25**, 4445–4451.

37 J. Zhang, H. Liu, Z. Wang and N. Ming, *Adv. Funct. Mater.*, 2007, **17**, 3295–3303.

38 S. Tan, A. Argondizzo, J. Ren, L. Liu, J. Zhao and H. Petek, *Nat. Photonics*, 2017, **11**, 806–812.

39 B. H. Li, C. E. Sanders, C. K. Shih, C. Wu, C. Y. Wang, G. Shvets, H. Y. Chen, J. Kim, L. J. Chen and M. Y. Lu, *Science*, 2012, **337**, 450–453.

40 J. Zhao, H. Sun, S. Dai, Y. Wang and J. Zhu, *Nano Lett.*, 2011, **11**, 4647–4651.

41 Y. D. Kim, H. Kim, Y. Cho, J. H. Ryoo, C.-H. Park, P. Kim, Y. S. Kim, S. Lee, Y. Li, S.-N. Park, Y. S. Yoo, D. Yoon, V. E. Dorgan, E. Pop, T. F. Heinz, J. Hone, S.-H. Chun, H. Cheong, S. W. Lee, M.-H. Bae and Y. D. Park, *Nat. Nanotechnol.*, 2015, **10**, 676–682.

42 S. K. Cushing, C. J. Chen, C. L. Dong, X. T. Kong, A. O. Govorov, R. S. Liu and N. Wu, *ACS Nano*, 2018, **12**, 7117–7126.

43 M. L. Brongersma, N. J. Halas and P. Nordlander, *Nat. Nanotechnol.*, 2015, **10**, 25–34.

44 K. H. Li, X. Liu, Q. Wang, S. Zhao and Z. Mi, *Nat. Nanotechnol.*, 2015, **10**, 140–144.

45 H.-Z. Chen, J.-Q. Hu, S. Wang, B. Li, X.-Y. Wang, Y.-L. Wang, L. Dai and R.-M. Ma, *Sci. Adv.*, 2017, **3**, e1601962.

46 H. Qian, S.-W. Hsu, K. Gurunatha, C. T. Riley, J. Zhao, D. Lu, A. R. Tao and Z. Liu, *Nat. Photonics*, 2018, **12**, 485–488.

47 W. Zhu, T. Xu, H. Wang, C. Zhang, P. B. Deotare, A. Agrawal and H. J. Lezec, *Sci. Adv.*, 2017, **3**, e1700909.

48 V. J. Sorger, R. F. Oulton, J. Yao, G. Bartal and X. Zhang, *Nano Lett.*, 2009, **9**, 3489–3493.

49 V. Caligiuri, M. Palei, G. Biffi, S. Artyukhin and R. Krahne, *Nano Lett.*, 2019, **19**, 3151–3160.

50 W. Wei, X. Yan and X. Zhang, *Sci. Rep.*, 2016, **6**, 33063.